15

n-Type β-$FeSi_2$/p-type Si Near-infrared Photodiodes Prepared by Facing-targets Direct-current Sputtering

Mahmoud Shaban[1] and Tsuyoshi Yoshitake[2]
[1]*Sauth Valley University,*
[2]*Kyushu University,*
[1]*Egypt*
[2]*Japan*

1. Introduction

Light detection in the near-infrared (NIR) region is an important issue in long distance optical fiber communication systems, local area networks, and optical interconnections in high speed computers. In recent years, the development of devices that are compatible with silicon electronic-photonic integrated circuits and can be operated at the telecommunication wavelengths of 1.3 and 1.55 μm has been the subject of intense research. The majority of optical fiber transmission systems operate at these wavelengths in order to take advantage of the low loss and low dispersion characteristics of silica-based optical fibers at these wavelength windows. Therefore, extraordinary technological innovations are increasingly adopted within the telecommunication industry as means of developing optoelectronic devices which operate at these wavelengths and are compatible with the current silicon technology (Kang et al, 1984; Luray et al, 2003; Masini et al, 2008). The key requirements for future integrated optoelectronics are light sources and light detectors that operate at the desired wavelength range and are compatible with the current Si technology.

The iron disilicide phase, β-$FeSi_2$, that can be grown on Si with 2%–5% lattice mismatch, is one of the best candidates for NIR photo-detection owing to several merits: (i) a large absorption coefficient, which is at least two orders of magnitude greater than that of crystalline silicon at 1.5 eV; (ii) a direct band gap of 0.85 eV; (iii) compatibility with Si technology; (iv) abundance of its elements (Fe and Si) in earth's crust; and (v) ecologically friendly material due to its non-toxicity. Therefore, β-$FeSi_2$ is a prime candidate material for optoelectronic and photovoltaic applications.

Various deposition methods such as; ion beam synthesis (Leong et al, 1996), reactive deposition epitaxy (Suemasu et al, 2000), and molecular beam epitaxy (Mahan et al, 1990) have been adapted for the growth of β-$FeSi_2$. However, thermal treatments such as annealing at temperatures greater than 800 °C are generally carried out after film deposition. This causes an easy condensation of β-$FeSi_2$ due to its high surface energy as compared to that of Si, which leads to a discontinuous surface structure. In addition, Fe atoms diffuse into Si. Although the solid solubility of Fe in Si is known to be low, for example, 2×10^{15} cm^{-3} at 900 °C, the diffusion coefficient is extremely large. This prevents the construction of β-

$FeSi_2$/Si heterojunctions with sharp interfaces. Fe atoms migrated into a depletion layer within Si, thereby producing a leak current. To overcome this problem, the template method has been suggested in which a thin template layer is grown at a low temperature before the general film fabrication procedure (Liu et al, 2004; Suemasu et al, 1999). We suggest another method in which thin films are epitaxially as-grown at a substrate temperature of 600 °C without annealing. Both the diffusion coefficient and the solid solubility of Fe in Si at 600 °C are a fifth to a tenth of those at 800 °C (Kendall & Devries, 1969).

Sputtering methods have been applied for a variety of film preparations and is easily available for industrial applications. In this study, we have adapted a facing-targets direct-current sputtering (FTDCS) method, in which a couple of targets are positioned in parallel and the substrate is set in the direction perpendicular to the two targets. As compared to the ordinary sputtering method, FTDCS has the following features due to a magnetic field between the targets: (i) high plasma density, (ii) less damage, (iii) fewer rises in substrate temperature, and (iv) lower stoichiometric difference from a target since the substrate is free of the plasma. On the other hand, species arriving at the substrate have a kinetic energy of several electron-volts; this value is larger than those observed in other preparation methods such as molecular beam epitaxy. These are suitable for growing β-$FeSi_2$ directly at low substrate temperatures by providing both Fe and Si by using $FeSi_2$ alloy targets.

2. Experimental procedure

Sputtering has proven to be a successful method of coating a variety of substrates with thin films of electrically conductive or non-conductive materials. One of the most striking characteristics of sputtering is its universality. Since the coating material is passed into the vapor phase by a mechanical rather than a chemical or thermal process, virtually any material can be deposited. Generally, direct current (DC) is used to sputter conductive materials, while radio frequency (RF) is used for non-conductive materials.

FTDCS apparatus is configured such that a pair of targets is mounted facing each other separated by a prespecified distance away from each other. A magnetic field extending in the space between the targets, called a discharge space, from one target to the other is provided by two permanent magnets, as shown in Fig. 1(a). The magnetic field flux, which has a perpendicular direction to the target surfaces, uniformly surrounds the discharge space to confine plasma within this space and to form a film on a substrate disposed at a position beside the discharge space under vacuum condition. The DC plasma can be adjusted over a wide range to control the deposition rate. The DC power supply supplies sputtering power to the apparatus while the shields of the vacuum chamber walls serve as an anode (ground) and the targets serve as a cathode (Kadokura, 2005).

The film preparation chamber is evacuated by means of an evacuation system, consisting of turbo-molecular pump connected to a rotary pump. A sputtering gas, such as argon, is introduced into the vacuum chamber through a gas inlet by a gas flow rate control system. Generally, inert gases are usually employed as the sputtering gas because they tend not to react with the target material or combine with any process gases and because they produce higher sputtering and deposition rates due to their high molecular weight. The sputtering plasma affects sputtering of the targets, thereby forming a thin film with composition corresponds to that of the targets on the substrate, as shown in Fig. 1(b). The sputtering plasma accelerates ionization of the sputtering gas, thereby increasing the sputtering rate and thus forming a film on the substrate at high deposition rates.

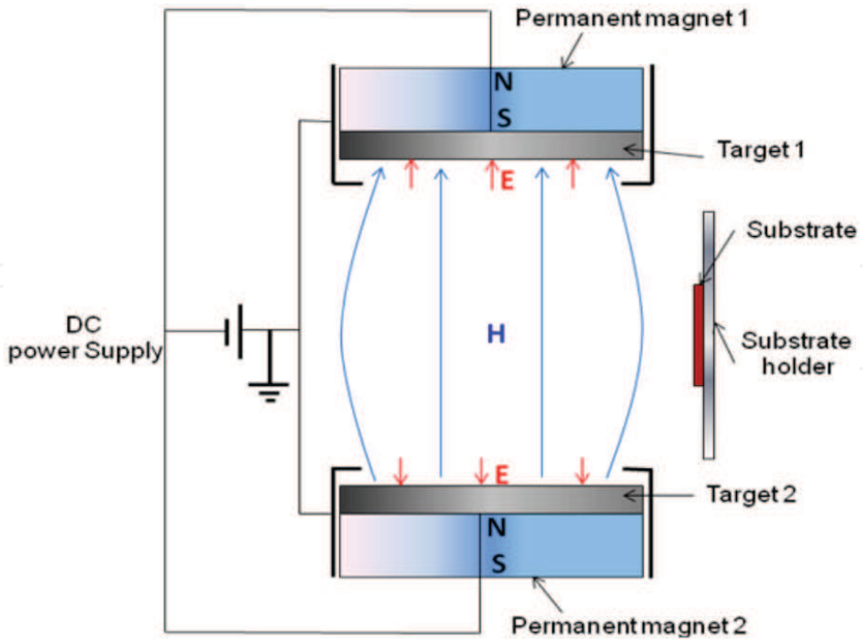

(a)

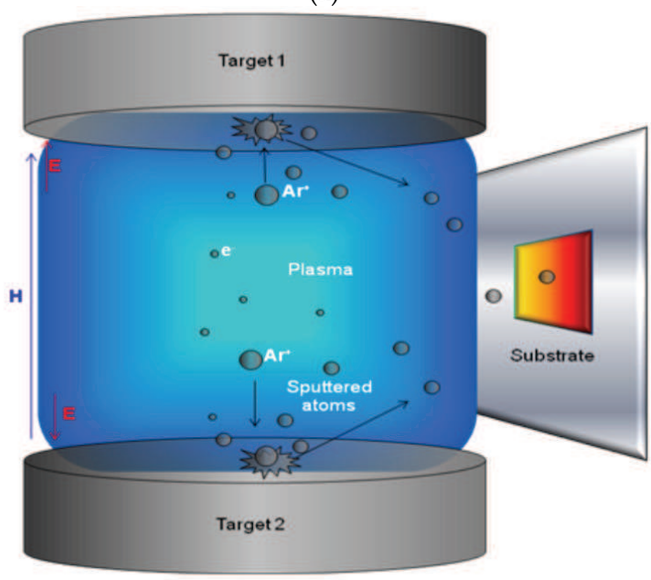

(b)

Fig. 1. Illustrations of; (a) FTDCS configuration, and (b) sputtering mechanism in FTDCS apparatus

The experiment procedure can be summarized as follows: β-FeSi$_2$ thin films of thickness 300 nm were deposited on Czochralski Si(111) substrates (resistivity: 10 Ω cm) of thickness 100 μm using FeSi$_2$ targets (purity: 4 N) with atomic ratio of Fe : Si = 1 : 2. The substrates were placed in the film preparation chamber after their native oxide layers were etched in dilute HF solution (1% HF). The chamber, which was equipped with a turbo-molecular pump, was evacuated to a base pressure of less than 1×10^{-5} Pa. Ar gas (purity: 6 N) was introduced into the chamber at a flow rate of 15 SCCM (SCCM denotes standard cubic centimeter per

minute). The β-$FeSi_2$ films were deposited at a constant pressure of 1.33×10^{-1} Pa. The operating DC voltage and current were 1 KV and 1.5 mA, respectively. After the β-$FeSi_2$ films were deposited at the substrate-temperature of 600 °C, they were transferred to a radio-frequency magnetron sputtering apparatus where Pd and Al electrodes were deposited on the top (Si) and bottom (β-$FeSi_2$) surfaces of the films, respectively. The electrodes were deposited at room temperature. The formation of Pd/β-$FeSi_2$ and Al/Si ohmic contacts were experimentally confirmed.

The structural characteristics of the prepared β-$FeSi_2$/Si heterojunctions were investigated by x-ray diffraction (XRD) measurements (Rigaku, RINT-2000/PC) and scanning electron microscopy (SEM) observations (JEOL, JSM-6340F). The optical properties were measured by a spectrometer (JASCO, V-570) with an integrating sphere (JASCO ISN-470) in the photon energy range of 0.6–1.2 eV. The current-voltage (*I-V*) characteristics were measured (Keithley, source-meter 2400) in the dark and under illumination by a 6 mW laser diode (LD) (Neoark, TC20) at a wavelength of 1.31 μm. The photoresponse properties were measured using a Xe lamp (Ushio, UXL-300D) and a monochromator (Oriel 77250) with a focal length of 125 mm and a line density of 600 l/mm. The light intensity was calibrated using a commercial photodiode (Hamamatsu G8372–1).

3. β-$FeSi_2$ film characterization

3.1 Epitaxial growth

The epitaxial growth of β-$FeSi_2$ films on Si(111) was confirmed on the basis of the following: XRD measurements in a $2\theta-\theta$ scan mode, grazing incidence method (2θ scan; at a fixed incidence angle of 4°), φ-scan and pole figure analysis. Figure 2 shows a typical $2\theta-\theta$ XRD pattern of β-$FeSi_2$ films. An intense 220/202 peak and a weak 440/404 peak due to β-$FeSi_2$ were observed near the 111 and 222 peaks of the Si substrate, respectively. No peaks were observed in the 2θ-scan measurement, thereby indicating the absence of polycrystalline elements in the film. Crystallites comprising the film are predominantly 101-oriented, which is similar to the β-$FeSi_2$ film epitaxially grown on Si(111) by chemical vapor deposition (CVD) (Akiyama et al, 2001). The full width at half maximum (FWHM) of the rocking curve corresponding to the 404 peak was 1.54°, as shown in the inset of Fig. 2.

The φ-scan measurement was performed in order to confirm the orientation of the crystalline plane parallel to the substrate plane. The rotation axis was normal to the substrate surface, that is, the [111] direction of the Si(111) substrate. The diffraction peaks due to the 422 planes for the Si substrate and 313 planes for the β-$FeSi_2$ film were detected in this measurement. The φ-scan diffraction patterns are shown in Fig. 3(a). The twin peaks due to β-$FeSi_2$-313 were observed between the Si-422 peaks; this indicates that three types of epitaxial variants were rotated at an angle of 120° with respect to each other (Akiyama et al, 2001). The epitaxial relationship is predominantly as follows:

$$\beta(101)/Si(111) \text{ with } \beta[101]//Si[0\,\bar{1}\,1]\,,\ [\bar{1}\,01], \text{ and } [\bar{1}\,10].$$

The pole figure, shown in Fig. 3(b), shows existence of the three types of epitaxial variants. The azimuth angles of two variants are equal, while the azimuth angle of the third variant is slightly shifted, owing to the orthorhombic crystallographic structure of β-$FeSi_2$ (Akiyama et al, 2001). It was confirmed that the β-$FeSi_2$ films were epitaxially grown not only in a direction perpendicular to but also in-plane with the Si(111) substrate.

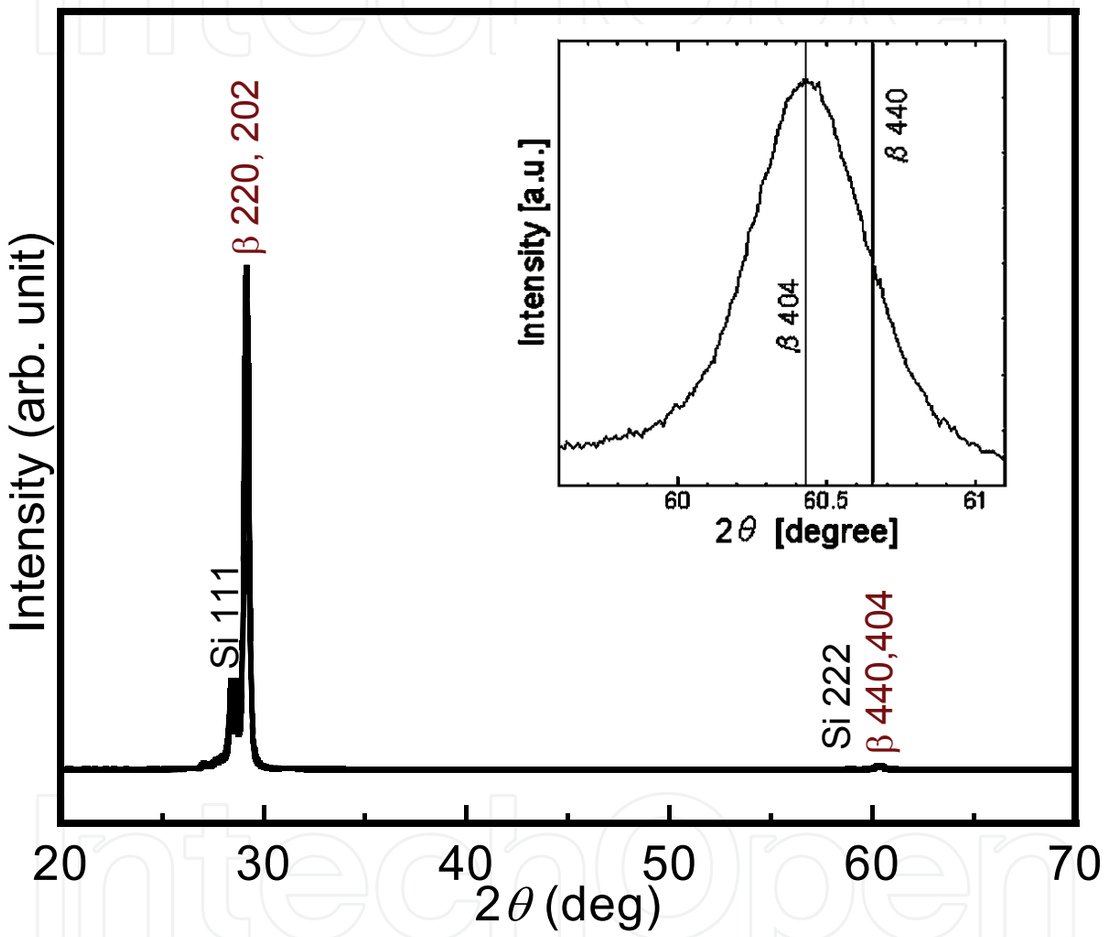

Fig. 2. X-ray diffraction pattern of the β-$FeSi_2$ thin film measured by a 2θ-θ method. The inset is the extension of β-404, 440 peaks.

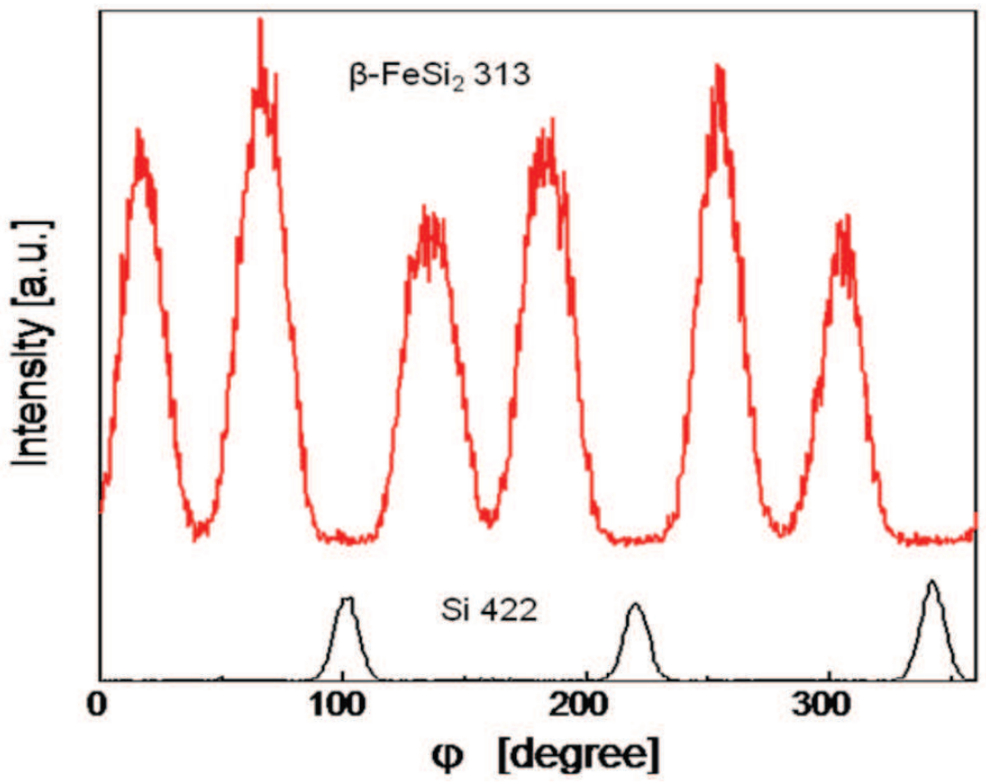

(a)

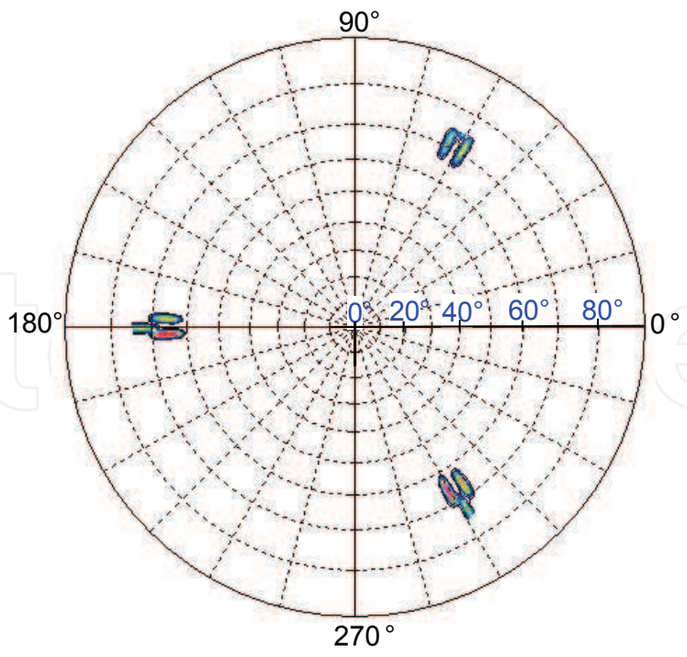

(b)

Fig. 3. (a) X-ray diffraction pattern of the β-$FeSi_2$ thin film measured by a φ-scan method; (b) pole figure plot of the 440/404 diffraction peak of β-$FeSi_2$

3.2 Optical characterization

The absorption coefficient is a strong function of the wavelength or photon energy. Near the absorption edge, the absorption coefficient for direct bandgap transitions can be expressed as;

$$\alpha \propto (hv - E_g)^{1/2}$$

where hv is the photon energy and E_g is the value of the bandgap. The absorption coefficient of β-$FeSi_2$ thin film, with thickness of 200 nm, was measured to be ~ 7×10^4 cm^{-1} at 1 eV. The interpolated indirect and direct optical band gaps were ~ 0.74 and 0.86 eV, respectively (Yoshitake et al, 2006). These values are in good agreement with those of the single crystalline bulk (Udono et al 2004). The absorption coefficient exceeds of 10^4 cm^{-1} for energies above 0.78 eV, which is close to the indirect optical bandgap of β-$FeSi_2$. From this measurement, the corresponding cut-off wavelength (λ_c) of photodiode devices with β-$FeSi_2$ thin film is expected to be ~1.55 μm.

Figure 4(a) shows the photoelectron spectrum of a β-$FeSi_2$ film. The threshold of the incident photon energy, which corresponds to the ionization potential of β-$FeSi_2$ (qV_{ip}), was measured to be 4.71 eV. From this value and the well-known parameters of Si and β-$FeSi_2$, the energy band diagram of the n-type β-$FeSi_2$/p-type Si heterostructure was derived, as shown in Fig. 4(b). Here, the Fermi level of β-$FeSi_2$ was assumed to be close to the conduction band because its high carrier density ranged from 10^{17} to 10^{18} cm^{-3} and its donor level was located only 20 meV below the conduction band (Yoshitake et al, 2006). The built-in potential (qV_{ip}) of the heterojunction was estimated to be ~ 0.9 eV. This value is sufficiently large for efficient photogenerated carrier collection in the heterojunction.

3.3 Electrical characterization

Figure 5 shows the temperature dependence of the electric conductivity of the film. The activation energy above 400 K was estimated to be around 0.41 eV, which corresponds to approximately half the optical band gaps. The Hall coefficient was negative, indicating n-type conduction. The activation energy between 280 and 320 K was estimated to be 0.02 eV. Since this corresponds to the energies between the donor level of Co and the bottom level of the conduction band (Tani et al, 1998), we believe that Co, which is a dominant impurity in the $FeSi_2$ target, are incorporated from the $FeSi_2$ target into the film. Although the carrier concentration was estimated to be approximately 10^{17} cm^{-3} at 300 K from the measured Hall coefficient and electric conductivity, the influence of the substrate on the electric conductivity of the film is not completely negligible. The carrier concentration might approximately lie between 10^{17} and 10^{18} cm^{-3} at 300 K (Yoshitake et al, 2006). It was confirmed that the deposited β-$FeSi_2$ was n-type since the heterojunction with p-type Si exhibited rectification current that is typically observed in a p-n junction. The conduction type of β-$FeSi_2$ is known to be dependent on the stoichiometry between Fe and Si. In this study, since the stoichiometric change from the targets to the film was estimated to be at a maximum of 1%, we believe that the Co incorporation from the targets is the primary reason for n-type conduction.

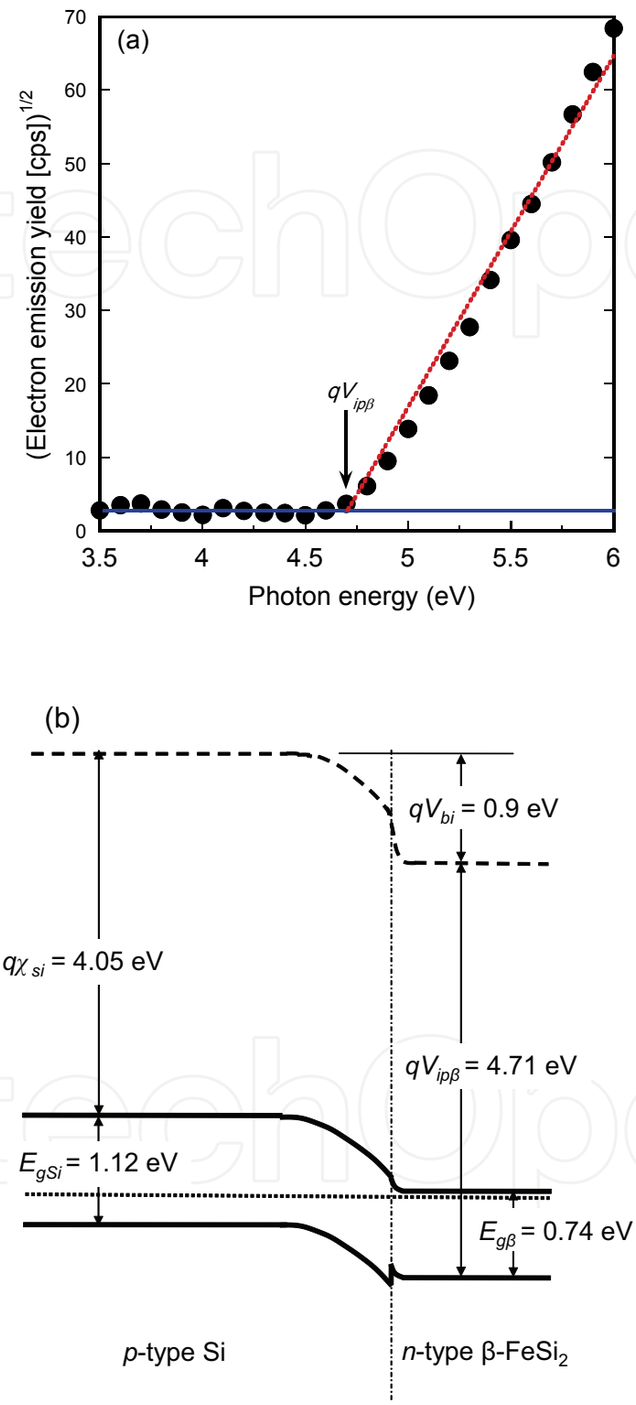

Fig. 4. (a) Photoelectron spectrum of a β-$FeSi_2$ film, wherein the threshold value of the photon energy corresponds to the ionization potential and (b) the energy band diagram of n-type β-$FeSi_2$/p-type Si heterojunction.

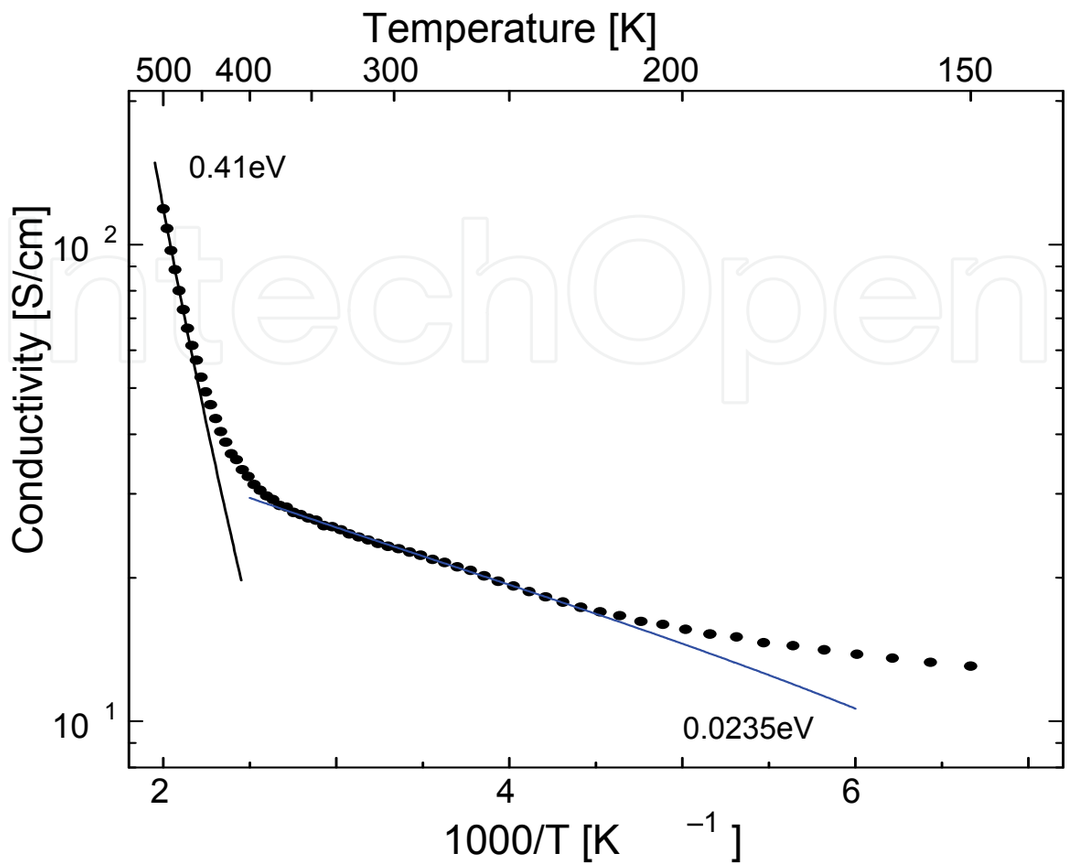

Fig. 5. Temperature dependence of the electric conductivity of the β-$FeSi_2$ film.

4. Device characterization

The fabricated device is a simple p–n heterostructure grown without annealing or passivation. Figure 6(a) illustrates a cross section schematic diagram of n-β-$FeSi_2$/p-Si heterojunction photodiode. The light is irradiated from front side of the Si substrate, which acts as the window material and helps in the epitaxial growth of crystalline β-$FeSi_2$. In this experiment we used Si substrates with thicknesses of 100 μm, however any smaller thickness can be used without affecting the device performance. Figure 6(b) shows a cross section SEM image in which a continuous and uniform β-$FeSi_2$ film without cracks was observed. In addition, the interface between the film and the substrate was extremely sharp which is essential to obtain good junction quality.

4.1 Current-voltage characteristics

Figure 7 shows the device characteristics measured in the dark and under the illumination of the 1.31 μm LD. The device exhibited good rectifying properties similar to those of conventional p-n junctions. The forward current was approximately two orders of magnitude greater than the reverse current. The dark leakage current at a reverse bias of –1 V was 5 μA, and this value increased to 20 μA at –5 V. The main source of the leakage current might be due to the Fe atoms that diffused from the β-$FeSi_2$ film to the Si substrate

during the film deposition process. The diffused atoms result in leakage centers and trap centers for the photogenerated carriers in addition to interface defects.
The measured photocurrent at zero bias was ~ 20 μA, and this value increased to 70 μA at –5 V. The ratio of the photocurrent to the dark leakage current at –1 V was approximately one order of magnitude. The current responsivity at zero bias was estimated to be ~ 3.3 mA/W. The inset of Fig. 3 shows the dynamic resistance deduced from the dark *I-V* characteristics. Because the major noise component at zero bias is mainly the Johnson noise, the device detectivity was estimated from the values of dynamic resistance and responsivity at zero bias. The shunt resistance, which corresponds to the dynamic resistance at zero bias, can be estimated to be approximately 50 kΩ from the inset. The detectivity at room temperature for the 1.31 μm illumination was estimated to be 1.5 ×10^9 cm √Hz W (Shaban et al, 2009a). This value is the largest in the previous β-$FeSi_2$ reports.

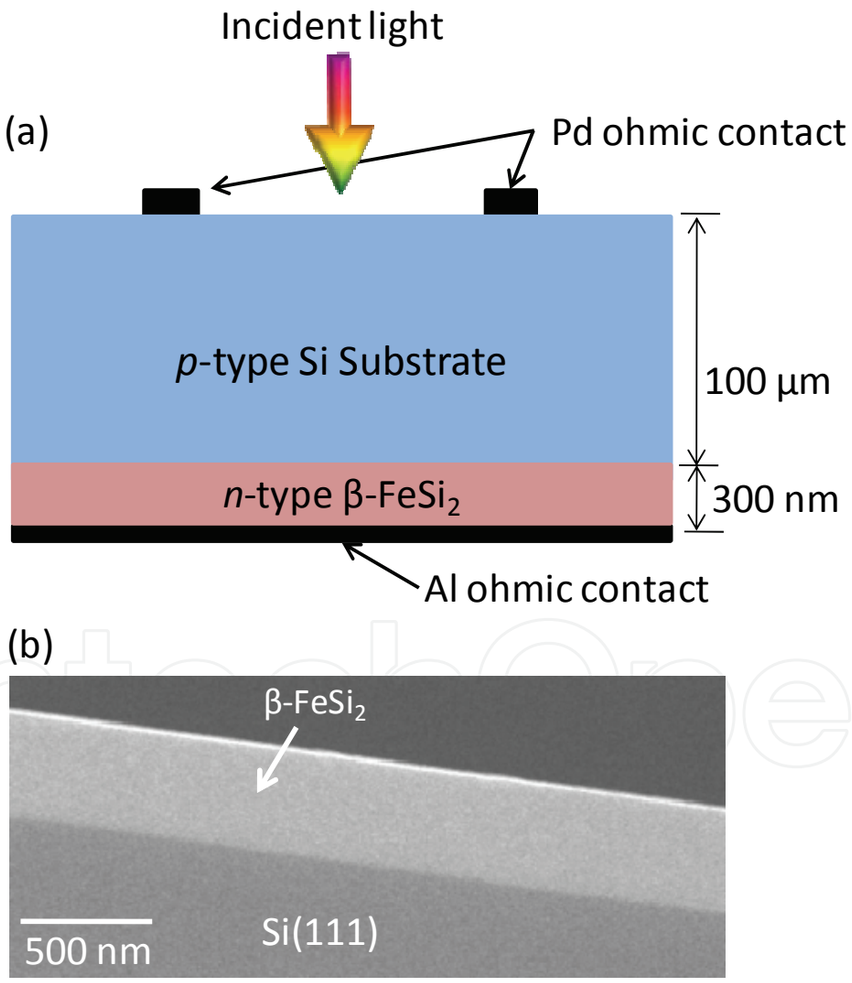

Fig. 6. (a) Schematic illustration of an n-type β-$FeSi_2$ (300 nm)/p-type Si (100 μm) heterojunction photodiode with Pd and Al electrodes on top (Si) and bottom (β-$FeSi_2$) surfaces, respectively. (b) Cross-sectional SEM image of β-$FeSi_2$ film deposited on Si(111) substrate.

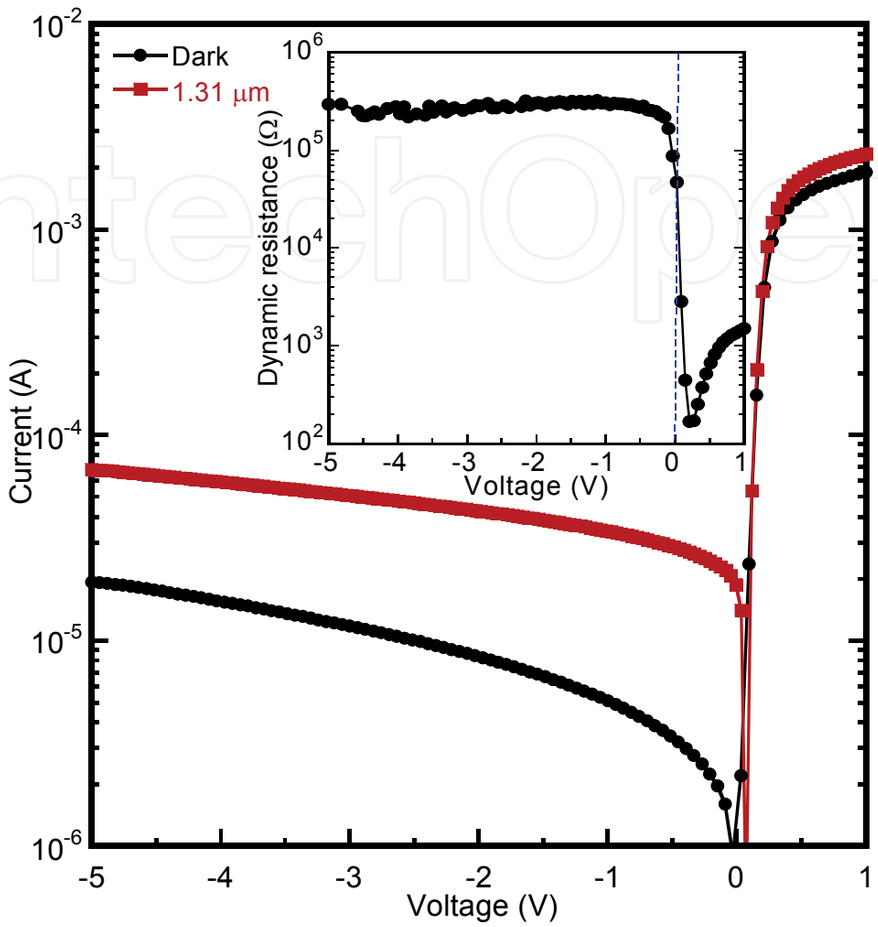

Fig. 7. *I-V* characteristics measured in the dark and under illumination with a 6 mW, 1.31 μm LD at room temperature. The inset shows the dynamic junction resistances deduced from the *I-V* characteristics.

4.2 Photoresponse spectrum

Figure 8 illustrates the photoresponse spectrum measured in the NIR range at zero bias and room temperature. The device evidently exhibited photoresponse beyond the Si cut-off wavelength up to the wavelength (approximately 1.5 μm) corresponding to the bandgap of β-FeSi$_2$. The inset of Fig. 4 shows the external quantum efficiency as a function of the reverse bias at 1.31 μm. The efficiency increased from 0.32% to 1.07% with an increase in the reverse bias from zero to –5 V. The reduction in the efficiency is attributed to light reflection and photocarrier recombination at the β-FeSi$_2$/Si interface. Further improvement in the device performance is expected to be achieved by reducing the surface reflection and passivation of the heterojunction interfaces in addition to suppressing the leakage current.

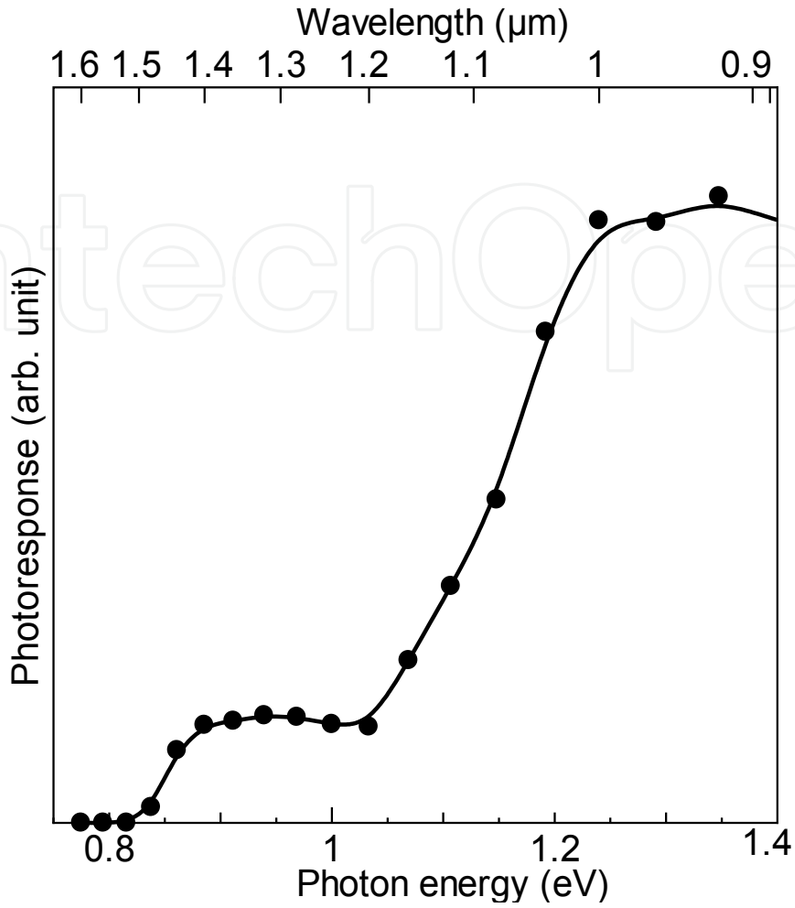

Fig. 8. Photoresponse spectrum of β-$FeSi_2$/Si heterojunction photodiode measured in the NIR range at zero bias and room temperature.

4.3 β-$FeSi_2$/Si photodiode with leakage-blocking layer

In order to improve the device performance, the leakage current should be reduced. This was achieved by inserting intrinsic-Si (*i*-Si) layer between the β-$FeSi_2$ film and Si substrate. Therefore, thin intrinsic-Si layers (thickness: 300 nm) were homoepitaxially grown on Czochralski-Si(111) substrates (resistivity: 10 Ω cm) at a substrate temperature of 700 °C. β-$FeSi_2$ layers (thickness: 300 nm) were successively grown on the Si layers at a substrate temperature of 600 °C by the FTDCS method. After that, the samples were transferred to a radio-frequency magnetron sputtering apparatus for depositing electrodes.

Figure 10(a) shows the *I-V* characteristics of the n-type β-$FeSi_2$/intrinsic-Si/p-type Si photodiodes, with an area of 3 mm^2, measured in the dark and under the illumination of the 6-mW 1.31 μm laser. The device exhibited good rectifying behavior with a rectifying ratio of greater than two orders of magnitude (Shaban et al, 2009b). The leakage current did not saturate and increased monotonously with the reverse voltage until the device experienced a thermal breakdown. Owing to the *i*-Si layer, the leakage current measured in this device was less than that measured in n-type β-$FeSi_2$ /p-type Si photodiodes (Shaban et al, 2009a).

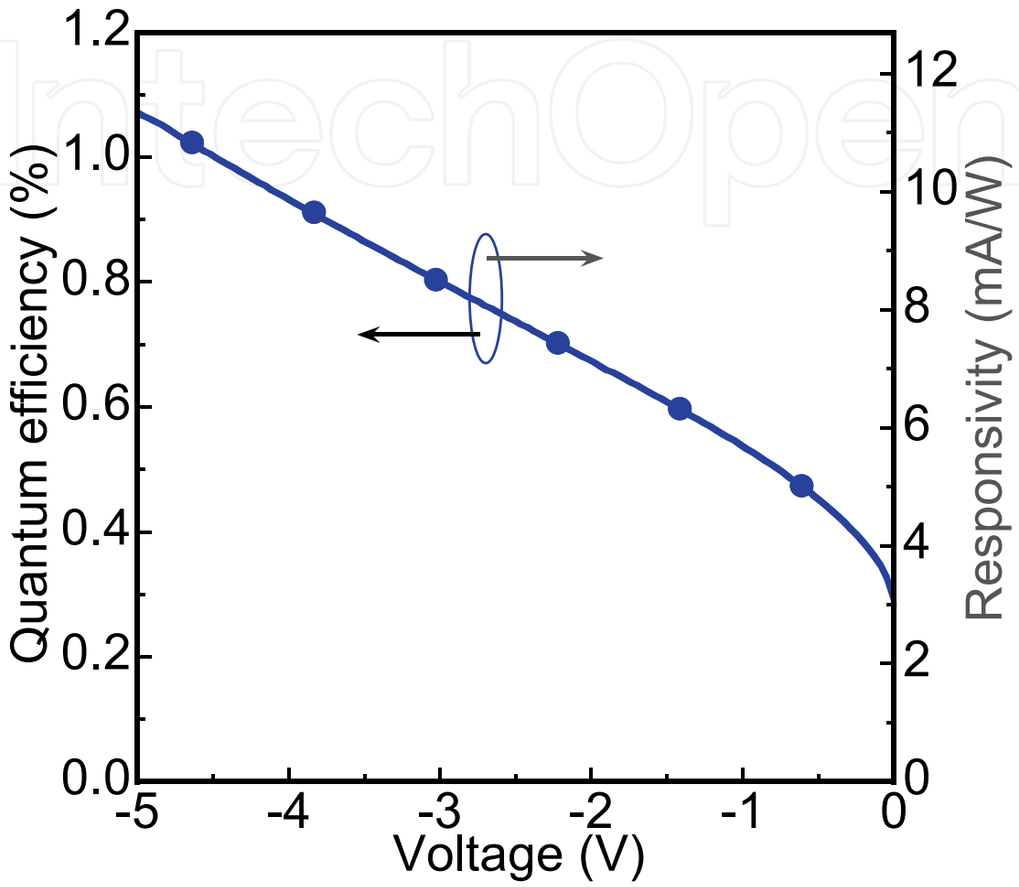

Fig. 9. Quantum efficiency and current responsivity of β-$FeSi_2$/Si heterojunction photodiode plotted against reverse bias under illumination with a 6 mW, 1.31 μm.

The photocurrent, resulted from the 1.31-μm illumination, increased from 40 to 840 μA with an increase in the reverse voltage from 0 to 5 V. The ratio of the photocurrent to the dark leakage current over the entire measured range of reverse voltages was approximately two orders of magnitude (Shaban et al, 2009b). The current responsivity increased from 6.6 to 140 mA/W with the increase in the reverse voltage from 0 to 5 V, as shown in Fig. 10(b). The Johnson-noise limited detectivity, which was measured at 1.31 μm and 300 K, was deduced to be 2.8×10^9 cm√Hz/W. This indicated the ability of the diode to detect light in the NIR region at room temperature.

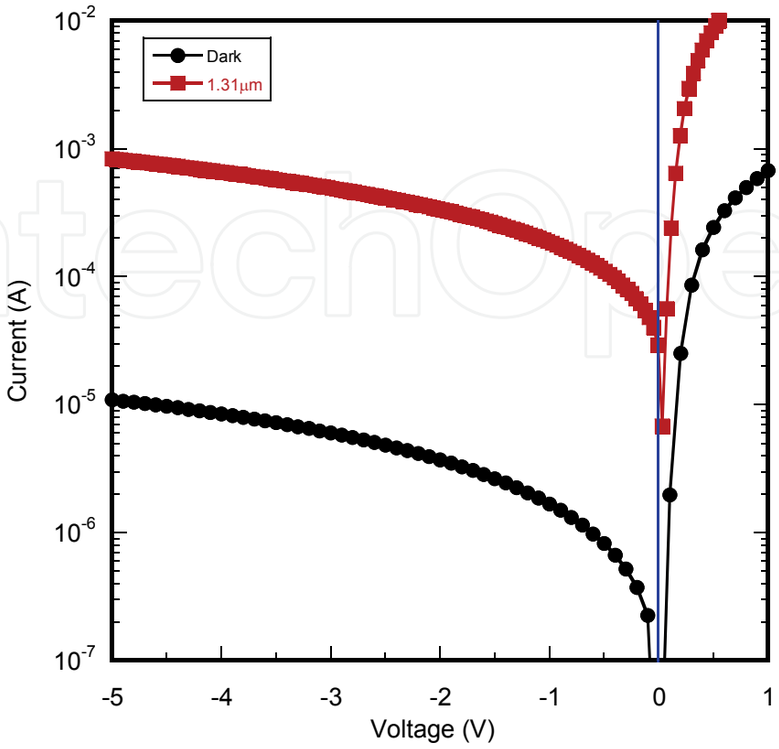

(a)

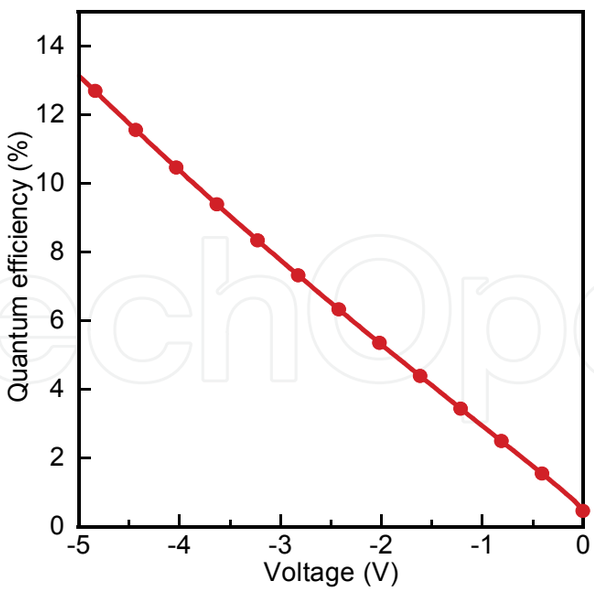

(b)

Fig. 10. (a) *I-V* characteristics of a heterojunction measured in the dark and under the illumination of a 6-mW 1.31 μm laser at 300 K. (b) External quantum efficiency vs reverse voltage measured under illumination at a wavelength of 1.31 μm.

5. Conclusions

A FTDCS method using $FeSi_2$ alloy targets, in which Fe and Si atoms are provided on the substrate at a low deposition rate comparable with that of molecular beam epitaxy, is a simple and successful method for the direct epitaxial growth of β-$FeSi_2$ thin films. The deposited β-$FeSi_2$ thin films show nearly the same optical and electric properties as the single crystalline bulk.

n-type β-$FeSi_2$/p-type Si heterojunctions in which the β-$FeSi_2$ layers were heteroepitaxially grown on Si(111) substrates with sharp interfaces were fabricated by FTDCS without carrying out postannealing. The band diagram of the heterostructure was derived, and the built-in potential was measured to be~ 0.9 V.

The *I-V* characteristics showed good rectifying properties with a shunt resistance of approximately 50 kΩ. The photoresponsivity under illumination at 1.31 μm was approximately 3.3 mA/W at room temperature. The specific detectivity was estimated to be 1.5×10^9 cm√HzW and the quantum efficiency, estimated at –5 V, was ~ 1.07%.

In order to improve the device performance, a leakage-blocking (*i*-Si layer) layer was suggested. The n-Type β-$FeSi_2$/*i*-Si/p-type Si heterojunction photodiodes showed an improved performance. They exhibited a current responsivity of 140 mA/W and quantum efficiency of 13% at –5 V.

The results suggest that these devices can operate efficiently at room temperature in the photoconductive mode and therefore they are promising candidates for NIR detectors that are compatible with Si.

6. References

Akiyama, K.; Ohya, S.; Takeno, H.; Kieda, N. & Funakubo, H. (2001). Growth of β-$FeSi_2$ Thin Film on Si (111) by Metal-Organic Chemical Vapor Deposition, In: *Jpn. J. Appl. Phys.*, Vol. 40, No. , pp.460-462.

Kadokura, S. (2005). Facing-targets-type sputtering apparatus and method, In : *U.S. Patent,* No. 6911123.

Kang, Y. ; Zadka, M. ; Litski, S. ; Sarid, G. ;Morse, M. ; Paniccia, M. J. ; Kuo, Y. H.; Bowers, J. ; Beling, A. ; Liu, H. D. ; McIntosh, D. C. ; Campbell, J. & Pauchard, A. (2008). Epitaxially-grown Ge/Si avalanche photodiodes for 1.3 microm light detection, In : *Optics Express*, Vol. 16, No. , pp. 9365-9368.

Kendall, D. L& Devries, D. B. (1969). Diffusion in silicon, In: *Semiconductor Silicon*, edited by R. R. Haberecht and E. L. Kern, Electrochemical Society, pp. 358-421, New York.

Leong, D. N.; Harry, M. A.; Reeson, K. J. & Homewood, K. P. (1996). On the origin of the 1.5 μm luminescence in ion beam synthesized β-$FeSi_2$. In: *Appl. Phys. Lett.*, Vol. 68, No. , pp. 1649-1651.

Luryi, S. ; Kastalsky, A. & Bean, J. C. (1984). New infrared detector on silicon chip, In : *IEEE Trans. Electron Devices*, Vol. 31, No. , pp.1135–1139.

Mahan, J. E.; Geib, K. M. & Robinson, G. Y. (1990). Epitaxial films of semiconducting $FeSi_2$ on (001) silicon, In : *Appl. Phys. Lett.*, Vol. 56, pp. 2126.

Masini, G. ; Colace, L. & Assanto, G. (2003). 2.5 Gbit/s polycrystalline germanium-on-silicon photodetector operating from 1.3 to 1.55 μm, In : *Appl. Phys. Lett.*, Vol. 82, No. , pp. 2524-2526.

Ootsuka, T. ; Fudamoto, Y. ; Osamura, M. ; Suemasu, T. ; Makita, Y. ; Fukuzawa, Y. & Nakayama, Y. (2007). Photoresponse properties of Al/n-β-$FeSi_2$ Schottky diodes using β-FeSi2 single crystals, In : *Appl. Phys. Lett.*, Vol. 91, No. 142114.

Shaban, M.; Nakashima, K.; Yokoyama, W. & Yoshitake, T. (2007). Photovoltaic Properties of n-type β-FeSi2/ p-type Si Heterojunctions, In : *Jpn. J. Appl. Phys.*, Vol. 46, pp. 667-669.

Shaban, M.; Nomoto, K.; Izumi, S. & Yoshitake, T. (2009a). Characterization of near-infrared n-type β-$FeSi_2$ /p-type Si heterojunction photodiodes at room temperature, *Appl. Phys. Lett.*, Vol. 94, No. 222113.

Shaban, M.; Izumi, S.; Nomoto, K. & Yoshitake, T. (2009b). n-Type β-$FeSi_2$/intrinsic-Si/p-type Si heterojunction photodiodes for near-infrared light detection at room temperature, *Appl. Phys. Lett.*, Vol. 95, No. 162102.

Suemasu, T.; Negishi, Y. ; Takakura, K. & Hasegawa, F. (2000). Room temperature 1.6 μm electroluminescence from a Si-Based light emitting diode with β-$FeSi_2$ active region, In: *Jpn. J. Appl. Phys.*, Vol. 39, pp. 1013-1015.

Tani J. & Kido, H. (1998). Electrical properties of Co-doped and Ni-doped β-$FeSi_2$, In: J. Appl. Phys., Vol. 84, pp. 1408-1410.

Udono, H.; Kikuma, I.; Okuno, T.; Matsumoto, Y.; Tajima, H. & Komuro, S. (2004). Optical properties of β-$FeSi_2$ single crystals grown from solutions, In: Thin Solid Films, Vol. 461, pp. 182-187.

Yoshitake, T.; Inokuchi, Y.; Yuri, A. & Nagayama, K. (2006). Direct epitaxial growth of semiconducting β-$FeSi_2$ thin films on Si(111) by facing targets direct-current sputtering, In: *Appl. Phys. Lett.*, Vol. 88, No. 182104.

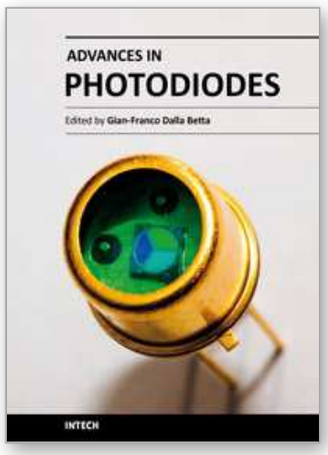

Advances in Photodiodes

Edited by Prof. Gian Franco Dalla Betta

ISBN 978-953-307-163-3
Hard cover, 466 pages
Publisher InTech
Published online 22, March, 2011
Published in print edition March, 2011

Photodiodes, the simplest but most versatile optoelectronic devices, are currently used in a variety of applications, including vision systems, optical interconnects, optical storage systems, photometry, particle physics, medical imaging, etc. Advances in Photodiodes addresses the state-of-the-art, latest developments and new trends in the field, covering theoretical aspects, design and simulation issues, processing techniques, experimental results, and applications. Written by internationally renowned experts, with contributions from universities, research institutes and industries, the book is a valuable reference tool for students, scientists, engineers, and researchers.

How to reference

In order to correctly reference this scholarly work, feel free to copy and paste the following:

Mahmoud Shaban and Tsuyoshi Yoshitake (2011). n-Type β-FeSi2/p-type Si Near-infrared Photodiodes Prepared by Facing-targets Direct-current Sputtering, Advances in Photodiodes, Prof. Gian Franco Dalla Betta (Ed.), ISBN: 978-953-307-163-3, InTech, Available from: http://www.intechopen.com/books/advances-in-photodiodes/n-type-fesi2-p-type-si-near-infrared-photodiodes-prepared-by-facing-targets-direct-current-sputterin

INTECH
open science | open minds

InTech Europe
University Campus STeP Ri
Slavka Krautzeka 83/A
51000 Rijeka, Croatia
Phone: +385 (51) 770 447
Fax: +385 (51) 686 166
www.intechopen.com

InTech China
Unit 405, Office Block, Hotel Equatorial Shanghai
No.65, Yan An Road (West), Shanghai, 200040, China
中国上海市延安西路65号上海国际贵都大饭店办公楼405单元
Phone: +86-21-62489820
Fax: +86-21-62489821

IntechOpen